Polarimetric 3D imaging in degraded environments

Kashif Usmani
Electrical and Computer Engineering Department, University of Connecticut, 371 Fairfield Road, Storrs, Connecticut 06269, USA
Timothy O'Connor
Biomedical Engineering Department, University of Connecticut, 260 Glenbrook Road, Unit 3247, Storrs, Connecticut, 06269, USA
Peter Marasco
Sensors Directorate, Air Force Research Laboratory, AFRL/RYMT 2241, Wright-Patterson AFB, Ohio 45433-7320, USA
Bahram Javidi
Electrical and Computer Engineering Department, University of Connecticut, 371 Fairfield Road, Storrs, Connecticut 06269, USA
Email: Bahram.Javidi@UConn.edu

Abstract

We investigate the performance of two-dimensional (2D) and three-dimensional (3D) polarimetric imaging in low illumination conditions and under partial occlusion using both visible range and long wave infrared (LWIR) range imaging sensors. Polarimetric imaging is an important imaging strategy within the fields of object visualization, object recognition, materials inspection, and materials classification. While relying on the light reflected from objects under study, polarimetric imaging can become challenging in degraded environments such as low illumination conditions or in the presence of partial occlusions. 3D integral imaging (InIm) is one prominent technique for improving scene visualization under such degraded conditions by using multiple perspectives of 2D elemental images of the scene to reconstruct the 3D image of the scene. This allows depth information to be extracted and improves the performance of low light image reconstruction due to being optimal in the maximum likelihood sense. Together, 3D polarimetric InIm can measure 3D polarimetric information of objects in photon-starved conditions and improve the performance of polarimetric imaging over conventional 2D techniques. Moreover, reconstructed 3D integral image at a particular depth or range under extremely low light environments may provide higher signal to noise ratio (SNR) as compared to the 2D images. In this paper, we present new data on the performance of visible range camera and long wave infrared (LWIR) imaging systems in the extraction of polarimetric information of objects in photon starved conditions. The polarimetric information of the object can be extracted from the Stokes parameters and degree of linear polarization (DoLP). The Stokes polarization parameters is measured using rotating polarizer in front of an image sensor and applied for the calculation of DoLP image of scene. An LWIR wire grid polarizer and a linear polarizer is used as the polarimetric objects in adverse environmental conditions for LWIR range and visible range imaging systems, respectively. Since the number of photons per pixel is very low in case of the visible range sensing system, the total variation (TV) denoising algorithm and mathematical restoration model are applied to the visible DoLP images to enhance the visualization. The mathematical model for signal restoration and TV denoising algorithm is not applied in case of the LWIR imaging system because enough thermal photons is present in the scene. A quantitative comparison on the performance of imaging systems in the extraction of polarimetric information for the object under adverse environmental conditions including low light conditions in terms of SNR is presented in this paper. The quantitative results demonstrate the effectiveness of the chosen preprocessing methods for visible range sensing and show overall better performance by the 3D integral imaging visible range sensing system in comparison to the LWIR imaging system. Finally, we compare the theoretical probability density function for the visible 2D and 3D DoLP images to the experimental histogram of visible 2D and 3D DoLP images. The result shows the strong similarity between the theoretically derived distributions and the probability distribution functions found through experimental measurements. These results demonstrate significantly better performance in visible range sensing for polarimetric 3D integral imaging over conventional 2D imaging in degraded environments.

1. Introduction

Polarimetric imaging is a technique that involves the measurement of polarimetric signature of reflected light from the object surface which contains the additional information of objects other than its intensity [1, 2]. Polarimetric signature of light reflected from an object surface can be used in target recognition, material inspection and material classification [3-5]. While depend on the light reflected from objects, the quality of polarimetric imaging suffers from noise in low light condition due to low signal to noise ratio and limited photons. Three-dimensional integral imaging can be used to improve the signal to noise ratio in low light conditions [6-8]. Polarization imaging with three-dimensional (3D) integral imaging has been reported for object visualization in low light illumination conditions [9-11]. Integral imaging is a three-dimensional imaging technique that records the multiple 2D images from different perspectives of 3D scene using a camera array, lenslet array or a single moving camera and reconstruct the 3D images computationally using these 2D images [12-20]. The advantage of 3D InIm is that it allows the depth information of 3D scene and improve the performance of low light imaging task. In addition, 3D InIm has the ability to reconstruct the objects behind occlusions [8].

In this paper, passive polarimetric information of 3D scene is extracted using 3D InIm in degraded environments of low light and under occlusion in visible and LWIR range. This paper is the extension of the work presented in [11]. In this paper, we have additionally considered the effect of occlusion in the scene under low light illumination and provided experiments and analysis accordingly. The polarimetric information of 3D scene is extracted by calculating nonlinear operator the degree of linear polarization (DoLP) using Stokes parameters. The captured images in low light conditions using visible sensor are significantly degraded by read noise, it becomes challenging to extract the polarimetric information in low light conditions using visible camera. In order to improve the visualization of visible polarimetric imaging in photon starved conditions, a mathematical restoration model [21] and total variation denoising [22] are applied. The mathematical model for signal restoration and TV denoising algorithm are not applied in case of the LWIR imaging system because enough thermal photons is present in the scene. Finally, the performance of polarimetric imaging in visible and LWIR range is compared in terms of SNR. The quantitative analysis of passive polarimetric integral imaging indicates that the performance of 3D integral imaging outperforms the conventional 2D imaging in degraded environments and the visible range imaging system produces higher SNR than the LWIR imaging system. Furthermore, the theoretical statistical distribution function of 2D DoLP and 3D DoLP is compared to the experimental histogram of 2D and 3D DoLP images in low light conditions. The theoretical probability density function (PDF) of 2D DoLP and 3D DoLP shows strong similarity to the experimental PDF of 2D DoLP and 3D DoLP images in low light conditions.

2. Polarimetric imaging

Polarization of light is characterized by the relationship between temporal average of magnitude and phase of two independent orthogonal electric field components. The optical properties of linear polarized light can be captured by inserting a rotating linear polarizer filter in front of image sensor as shown in Fig.1 [1, 2].

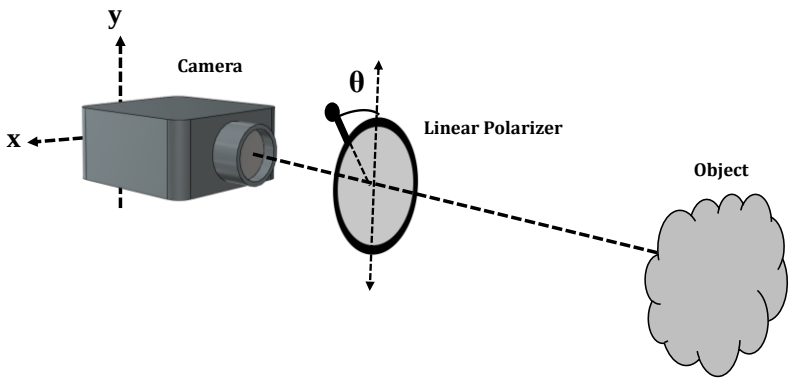

Fig.1 Experimental setup of polarimetric imaging system

The Stokes parameters are defined in terms of the intensity of light wave in Eq. (1) [2].

$$S_0 = I^{0^o} + I^{90^o}$$
$$S_1 = I^{0^o} - I^{90^o} \quad (1)$$
$$S_2 = I^{45^o} - I^{135^o},$$

where, I^{0^o}, I^{45^o}, I^{90^o} and I^{135^o} are the intensities of electric filed vector filtered with 0^o, 45^o, 90^o and 135^o linear polarizer filter, respectively. The polarimetric information of scene can be extracted by calculating the degree of linear polarization (DoLP) using Stokes parameters as [2];

$$\text{DoLP} = \frac{\sqrt{S_1^2 + S_2^2}}{S_0}, \quad (2)$$

where, S_i [i = 0, 1, 2] in the Eq. 2 are the Stokes parameters and the value of DoLP ranges from 0 to 1.

3. Polarimetric integral imaging

Integral imaging is a well-known technique for three-dimensional passive imaging. In this method, intensity as well as directional information of 3D scene is recorded by a camera array, lenslet array or a single camera on a moving platform [11-19]. The 2D images from multiple perspective of 3D scene recorded by camera sensors are known as elemental images. These multiple elemental images can be used to produce the 3D reconstruction of scene either computationally or optically. Figure 1 shows the diagram of scene capturing process using a single camera on a moving platform, and Fig. 1 (b) shows the 3D reconstruction process via synthetic aperture integral imaging (SAII) [20] using multiple 2D elemental images. The 3D scene is reconstructed by back propagating the captured elemental images through a virtual pinhole array to the desired depth. The 3D scene can be reconstructed at any depth that falls within the depth of field of captured elemental images. The advantages of using 3D integral imaging are that it uses parallax and depth reconstructed 3D images to reduce the effects of partial occlusions in front of the scene and to segment out objects of interest from the background. Moreover, reconstructed 3D integral image at a particular depth or range under extremely low light environments provides higher signal to noise ratio (SNR) as compared to the 2D images [8].

The reconstruction of polarimetric 3D scene at depth z can be computed as [20];

$$I_z^{\theta}(x,y) = \frac{1}{O(x,y)} \sum_{m=0}^{M-1} \sum_{n=0}^{N-1} \left[I_{m,n}^{\theta} \left(x - \frac{m \times L_x \times p_x}{c_x \times z / f}, y - \frac{n \times L_y \times p_y}{c_y \times z / f} \right) + \varepsilon \right]. \quad (3)$$

In the Eq.3 the (x, y) is the image pixel index, $O(x, y)$ is the overlapping pixel number on (x, y). $I^{\theta}_{m,n}$ is the set of polarimetric elemental images with multiple directions θ [0°, 45°, 90°, 135°] while the subscripts m, n represent the location of the elemental image. M and N are the total numbers of elemental images in the horizontal (H) and vertical (V) directions. L_x and L_y are the total number of pixels of elemental images and in the x and y directions. f is the focal length of camera c_x, and c_y are the sensor size in the x and y directions and ε is the additive noise of camera.

Three dimensional polarimetric integral imaging experiments were performed by a moving camera on two axes translational stages in low light and low light under partial occlusions. A linear polarizer filter in front of the camera was used to record a set of four images [$I^{0^{\circ}}$, $I^{45^{\circ}}$, $I^{90^{\circ}}$, $I^{135^{\circ}}$] by rotating the polarizer filter at angle θ (0°, 45°, 90°, 135°) with respect to the y-axis as shown in Fig.1. The 3D scene consists of a polarizer, a mannequin, and the test tubes filled with hot water to provide an IR source as shown in Fig. 2. The process of 3D polarimetric integral imaging using visible and LWIR range sensors were similar, the only difference is that linear polarizer film was used for visible polarization and IR wire grid polarizer was used for LWIR polarization as shown in Fig. 2. For fair comparison of visible and LWIR polarimetric images, the pixel size of visible camera is binned with 3 by 3 binning to 19.5μm×19.5μm. The pixel size of LWIR camera is 17μm×17μm.

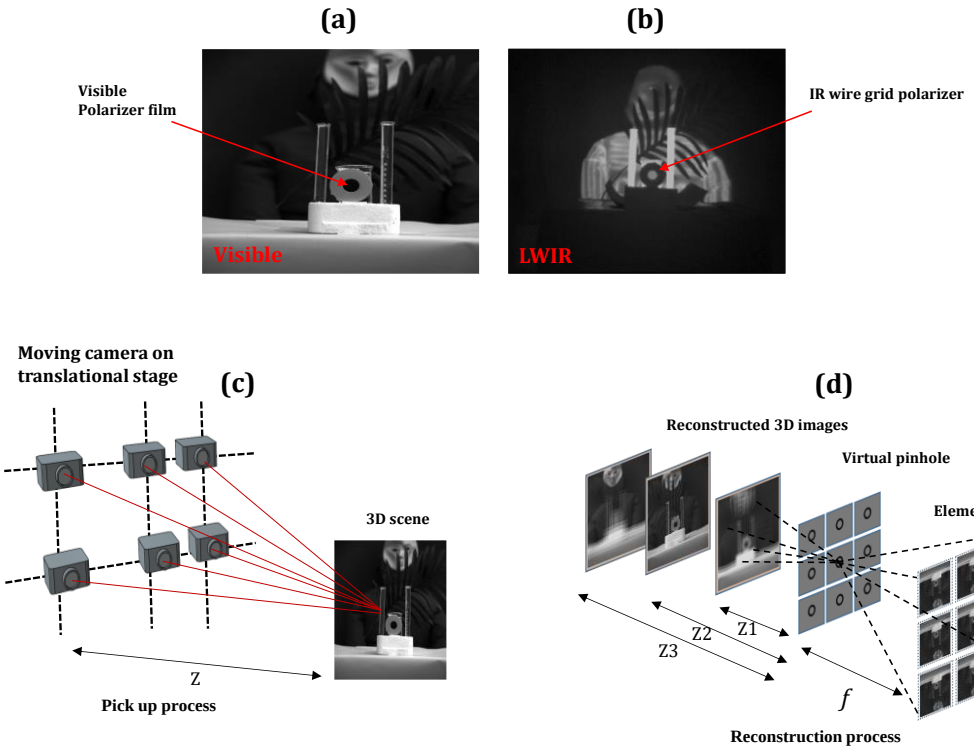

Fig. 2. (a) Reference image of 3D scene in high illumination using visible camera, (b) reference image of 3D scene using LWIR camera. (c-d) Integral imaging set up, (c) pickup process (d) reconstruction process via SAII.

4. Result and discussion

We recorded 9 (3×3) elemental images for SAII with a pitch size of 30mm in both horizontal and vertical directions using visible (Hamamatsu C11440-42U) and LWIR camera (Tamarisk 320 LWIR camera 60 Hz). The focal length of visible and LWIR cameras are 50mm and 11mm, respectively. The captured polarimetric images [$I^{0°}$, $I^{45°}$, $I^{90°}$, $I^{135°}$] with multiple orientations of polarization θ (0°, 45°, 90°, 135°) are used to calculate the Stokes parameters, and DoLP images using Eq. (1) and Eq. (2), respectively. Fig. 3 shows 2D and 3D DoLP images using visible camera in degraded conditions such as low illumination and low illumination under partial occlusion. The low light condition is calculated in terms of photons per pixel in case visible range camera. The photons per pixel under low light conditions prior to binning is estimated as 3.5 [10]. The captured images using visible camera in low light environments are embedded in noise due to low photon counts. The noise present in the captured images due to photon starved condition is enhanced during the calculation of nonlinear operator DoLP as shown in Fig. 3(a). The reconstructed 3D DoLP image reduces the saturation effect of noise as shown in Fig 3(b). The polarimetric information of scene in low light condition under partial occlusion is shown in Figs. 3(c-d). The occlusion infront of the scene as shown in Fig. 3(c) is reduced by 3D integral imaging. The reconstructed 3D DoLP image reduces the effect of partial occlusion in front of the scene and segment out the object of interest from the background as shown in Fig. 3(d).

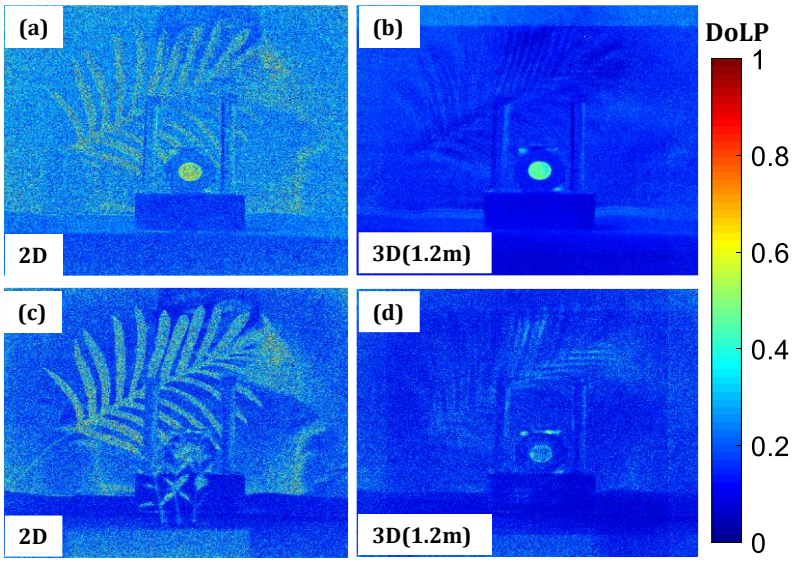

Fig.3. (a-b) Polarimetric images in low light illumination using visible range camera. (a) 2D DoLP image and (b) 3D DoLP image at z = 1.2m in low light illumination. (c-d) Polarimetric images in low light under partial occlusions using visible range camera. (c) 2D DoLP image and (d) 3D DoLP image at z = 1.2m in low light under partial occlusions. The estimated photons per pixel is 3.5.

Finally, a total variation (TV) denoising along with mathematical model of dehazing is applied to reduce the noise in polarimetric 2D DoLP and 3D DoLP images. The enhanced 2D and 3D DoLP images after preprocessing in low light and low light under occlusions are shown in Fig4. Fig. 4(a) and Fig. 4(b) show the noise free images of DoLP in low light condition for 2D and 3D case, respectively and Fig. 4(c) and Fig. 4(d) show the noise free 2D DoLP and 3D DoLP images in low light under occlusion, respectively.

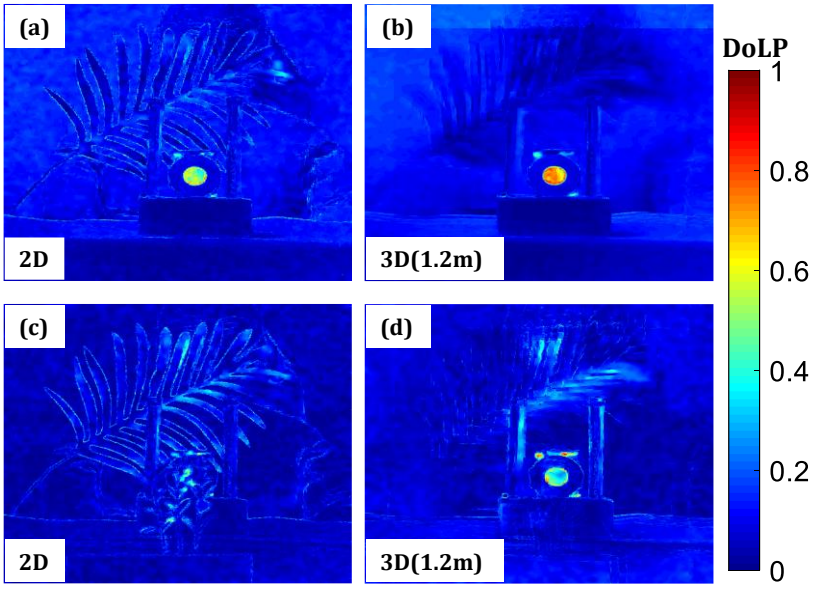

Fig.4. (a-c) Polarimetric images in low light illumination using visible range camera after TV denoising and dehazing. (a) 2D DoLP image and (b) 3D DoLP image at z = 1.2m in low light illumination. (c-d) Polarimetric images in low light under partial occlusions using visible range camera after TV denoising and dehazing. (c) 2D DoLP image and (d) 3D DoLP image at z = 1.2m in low light under partial occlusions.

The extraction of polarimetric information using LWIR camera is same as that of visible camera. The mathematical model for signal restoration and TV denoising algorithm is not applied in case of the LWIR imaging system because enough thermal photons is present in the LWIR scene. Fig. 5 shows the polarimetric images using LWIR camera in low light and partial occlusion conditions. Fig. 5(a) and Fig. 5(b) show the 2D and 3D LWIR polarimetric images in

low light conditions, respectively. Fig. 5(c) and Fig. 5(d) show the 2D and 3D LWIR polarimetric images in low light under partial occlusion, respectively.

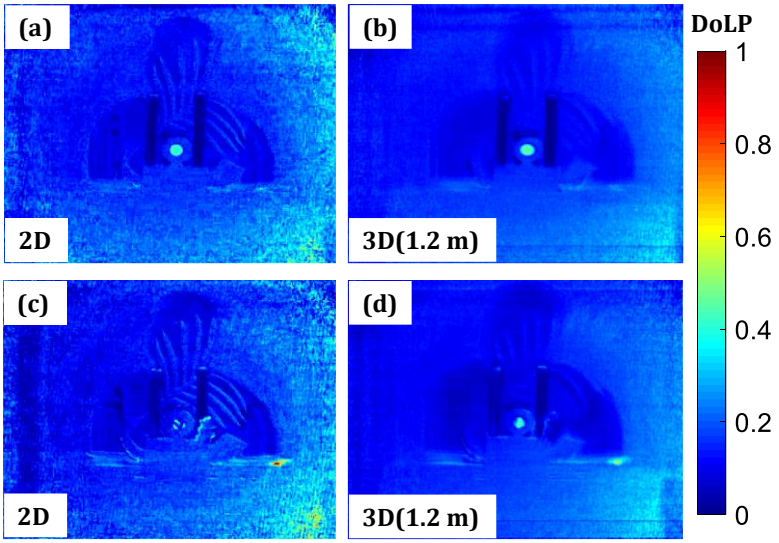

Fig.5. (a-c) Polarimetric images using LWIR range camera. (a) 2D DoLP image and (b) 3D DoLP image at z = 1.2m. (c-d) Polarimetric images in under partial occlusions using LWIR range camera. (c) 2D DoLP image and (d) 3D DoLP image at z = 1.2m under partial occlusions.

Finally, we compare the result of polarimetric images using visible and LWIR sensors by measuring the signal to noise ratio of polarimetric and non-polarimetric region. The SNR is defined as $\mathrm{SNR} = (\mu_s - \mu_b) \Big/ \sqrt{\sigma_s^2 + \sigma_b^2}$, μ_s and μ_b are the mean of polarimetric and non-polarimetric regions respectively, and σ_s and σ_b are the standard deviation of polarimetric and non-polarimetric regions respectively. The same area is selected from the DoLP images in case of visible and LWIR. The background region is chosen as the area which contains the lowest pixel value. Table 1 shows the quantitative comparison of polarimetric images using visible and LWIR sensors. The quantitative results indicate that 3D DoLP with preprocessing outperforms the 2D DoLP image with preprocessing in low light conditions. It also shows that the visible range imaging system with preprocessing produces higher SNR than the LWIR imaging system in DoLP calculation.

Table 1. SNR comparison of visible and LWIR polarimetric image in low light illumination

	Visible				**LWIR**	
	No processing		**After preprocessing**			
	2D DoLP	3D DoLP	2D DoLP	3D DoLP	2D DoLP	3D DoLP
SNR	1.85	5.29	10.97	23.91	2.19	2.70

The statistical analysis of 2D and 3D DoLP images are done by considering the visible 2D image in low light condition is dominated with camera read noise, which has a Gaussian distribution [11]. From Eq.1, the Stokes parameters which are the addition and subtraction of two orthogonal polarimetric images. Therefore, the calculated Stokes parameters are read noise dominated with Gaussian distribution with same variance and different means. The probability density function of visible DoLP [Eq.2] after considering Stokes parameters as Gaussian distribution follows the following distribution function [11].

$$f(\mathrm{P}) = \sum_{j=0}^{\infty}\sum_{k=0}^{\infty} \frac{\left(e^{-\frac{\delta}{2}}\left(\frac{\delta}{2}\right)^{j}\right)\left(e^{-\frac{\gamma}{2}}\left(\frac{\gamma}{2}\right)^{k}\right) \times 2\mathrm{P}^{1+2j}\left(1+\mathrm{P}^{2}\right)^{-3/2-j-k}}{j!k!B\left(1+j,1/2+k\right)}, \tag{4}$$

where, P represents the DoLP of the polarimetric object in low light, δ and γ represent the non-centrality parameters of doubly non central F-distribution. The non-centrality parameters are $\delta = \sum_{i=1}^{2} (\mu_i/\sigma)^2$ and $\gamma = (\mu_0$

/σ)^2, where μ_i and σ^2 are the mean and variance of Stokes parameters and i [0,1,2] is the index of Stokes parameter. B(.) represents the beta function with j and k are the summations variables [23].

The experimental histogram of polarimetric area of visible DoLP image in low light condition and the probability density function of DoLP using Eq.4 for 2D and 3D case are plotted in the Fig.6. The graphs in Fig.6 indicate that the theoretically probability density function for the 2D and 3D DoLP images are similar to the experimental histogram of 2D and 3D DoLP images. The probability density function for 3D DoLP has less standard deviation than 2D DoLP, which confirms that 3D DoLP has less noise compared to the 2D DoLP.

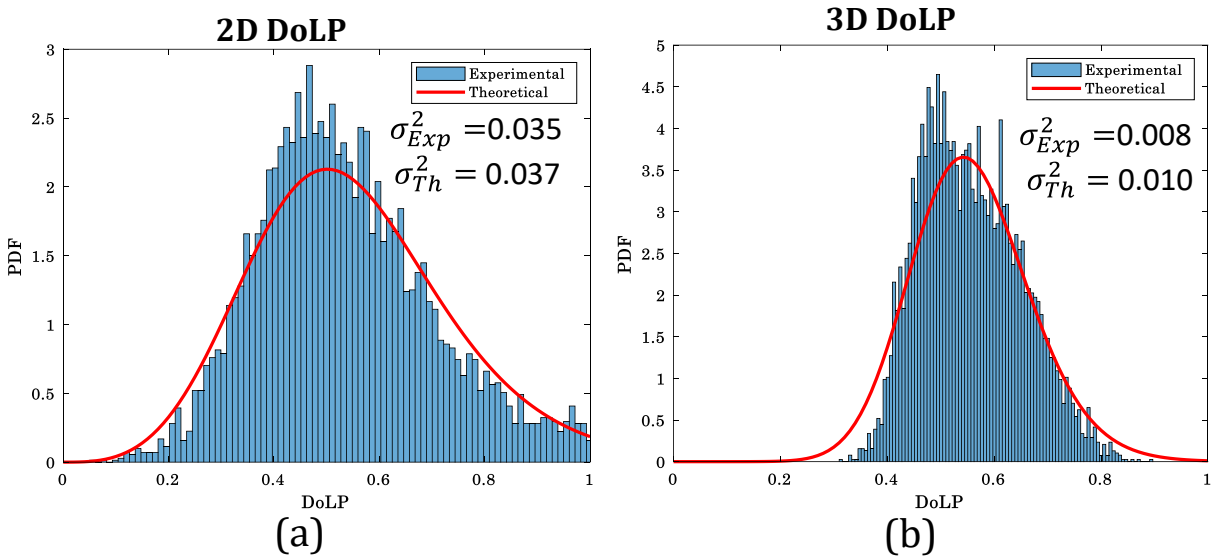

Fig. 6. Theoretical and experimental probability density function of visible DoLP images in low light illumination conditions (a) 2D DoLP image, and (b) 3D DoLP image. Red curve represent the theoretically derived PDF and blue histogram represent the experimental PDF.

5. Conclusions

In summary, we have compared the 3D polarimetric imaging of visible and LWIR range cameras in the adverse conditions of low light and partial occlusions. In order to extract the polarimetric information in low light condition using visible camera, mathematical model of restoration and TV denoising are used. The advantage of three-dimensional integral is that it reconstructs the object of interest in front of the partial occlusion and improve the performance of low light imaging task. The visible polarimetric imaging outperforms the LWIR polarimetric imaging in terms of SNR. Also, we derived theoretically the probability density function for the visible 2D and 3D DoLP images and show strong similarity between the theoretically derived distributions and the probability distribution functions found through experimental measurements. These results demonstrate significantly better performance in visible range sensing for polarimetric 3D integral imaging over polarimetric 2D imaging in degraded environments.

6. Funding

Air Force Office of Scientific Research (FA9550-18-1-0338, FA9550-21-1-0333); Office of Naval Research (N000141712405, N000142012690).

7. Acknowledgements

B. Javidi acknowledges support by Air Force Office of Scientific Research (FA9550-18-1-0338, FA9550-21-1-0333); Office of Naval Research (N000141712405, N000142012690), and Hamamatsu Photonics.

8. References

[1] G.P. Konnen, *Polarized light in nature* (Cambridge University, 1985).

[2] M. Born and E. Wolf, *Principles of Optics: Electromagnetic Theory of Propagation, Interference and Diffraction of Light* (Cambridge University, 1999).

[3] L. B. Wolff, "Polarization-based material classification from specular reflection," *IEEE Trans. Pattern Anal. Mach. Intell*. 12(11): 1059–1071 (1990).

[4] J. S. Tyo, D. L. Goldstein, D. B. Chenault, and J. A. Shaw, "Review of passive imaging polarimetry for remote sensing applications," Appl. Opt., 45(22): 5453–5469 (2006).

[5] K. T. Thilak, C. D. Creusere, and D. G. Voelz, "Passive polarimetric imagery-based material classification robust to illumination source position and viewpoint," IEEE Trans. Image Process. 20, 288–292 (2011).

[6] B. Tavakoli, B. Javidi, and E. Watson, "Three-dimensional visualization by photon counting computational integral imaging," Opt. Express **16**(7), 4426–4436 (2008).

[7] A. Stern, D. Aloni, and B. Javidi, "Experiments with three-dimensional integral imaging under low light levels," IEEE Photonics J. **4**(4), 1188–1195 (2012).

[8] A. Markman, X. Shen, and B. Javidi, "Three-dimensional object visualization and detection in low light illumination using integral imaging", Opt. Lett. **42**(16), 3068-3071 (2017).

[9] A. Carnicer and B. Javidi, "Polarimetric 3D integral imaging in photon starved conditions," Opt. Express **23**(5), 6408–6417 (2015).

[10] X. Shen, A. Carnicer, and B. Javidi, "Three-dimensional polarimetric integral imaging under low illumination conditions," Opt. Lett. **44**(13), 3230–3233 (2019).

[11] K. Usmani, T. O'Connor, X. Shen, P. Marasco, A. Carnicer, D. Dey, and B. Javidi, "Three-dimensional polarimetric integral imaging in photon-starved conditions: performance comparison between visible and long wave infrared imaging," Opt. Express **28**(13), 19281–19294 (2020).

[12] G. Lippmann, "Epreuves reversibles donnant la sensation du relief," J. Phys. 7(1), 821–825 (1908).

[13] S. H. Hong, J. S. Jang, and B. Javidi, "Three-dimensional volumetric object reconstruction using computational integral imaging," Opt. Express **12**(3), 483–491 (2004).

[14] B. Javidi, X. Shen, A. Markman, P.L. Carmona, A. Martinez-Uso, J. M. Sotoca, F. Pla, M. Martinez-Corral, G. Saavedra, Y. Huang, A. Stern, "Multidimensional Optical Sensing and Imaging System (MOSIS): From macroscales to microscales", Proc. IEEE **105**(5), 850-875 (2017).

[15] N. Davies, M. McCormick, and L. Yang, "Three-dimensional imaging systems: a new development," Appl. Opt. **27**(21), 4520–4528 (1988).

[16] F. Okano, H. Hoshino, J. Arai, and I. Yuyama, "Real-time pickup method for a three-dimensional image based on integral photography," Appl. Opt. **36**(7), 1598–1603 (1997).

[17] J. Liu, D. Claus, T. Xu, T. Keßner, A. Herkommer, and W. Osten, "Light field endoscopy and its parametric description," Opt. Lett. **42**(9), 1804–1807 (2017).

[18] J. Arai, E. Nakasu, T. Yamashita, H. Hiura, M. Miura, T. Nakamura, and R. Funatsu, "Progress overview of capturing method for integral 3-D imaging displays," Proc. IEEE 105(5), 837–849 (2017).

[19] M. Yamaguchi, "Full-parallax holographic light-field 3-D displays and interactive 3-D touch," Proc. IEEE 105(5), 947–959 (2017).

[20] J. S. Jang and B. Javidi, "Three-dimensional synthetic aperture integral imaging," Opt. Lett. 27(13), 1144–1146 (2002).

[21] C. Tang, Y. Wang, H. Feng, Z. Xu, Q. Li, and Y. Chen, "Low-light image enhancement with strong light weakening and bright halo suppressing," IET Image Process. **13**(3), 537–542 (2019).

[22] L. I. Rudin, S. Osher, and E. Fatemi, "Nonlinear total variation-based noise removal algorithms," Phys. D 60(1-4), 259–268 (1992).

[23] W. G. Bulgren, "On Representations of the Doubly Non-Central F Distribution," J. Am. Stat. Assoc. **66**(333), 184–186 (1971).